

# Coherent Spin-Current Oscillations in Transverse Magnetic Fields

Robin Steinigeweg,<sup>1,\*</sup> Stephan Langer,<sup>2</sup> Fabian Heidrich-Meisner,<sup>2</sup> Ian P. McCulloch,<sup>3</sup> and Wolfram Brenig<sup>1</sup>

<sup>1</sup>*Institute for Theoretical Physics, Technical University Braunschweig, D-38106 Braunschweig, Germany*

<sup>2</sup>*Department of Physics and Arnold Sommerfeld Center for Theoretical Physics, Ludwig-Maximilians-Universität München, D-80333 München, Germany*

<sup>3</sup>*School of Physical Sciences, The University of Queensland, Brisbane, QLD 4072, Australia*

(Dated: April 9, 2018)

We address the coherence of the dynamics of spin-currents with components transverse to an external magnetic field for the spin-1/2 Heisenberg chain. We study current autocorrelations at finite temperatures and the real-time dynamics of currents at zero temperature. Besides a coherent Larmor oscillation, we find an additional collective oscillation at higher frequencies, emerging as a coherent many-magnon effect at low temperatures. Using numerical and analytical methods, we analyze the oscillation frequency and decay time of this coherent current-mode versus temperature and magnetic field.

PACS numbers: 05.60.Gg, 71.27.+a, 75.10.Jm

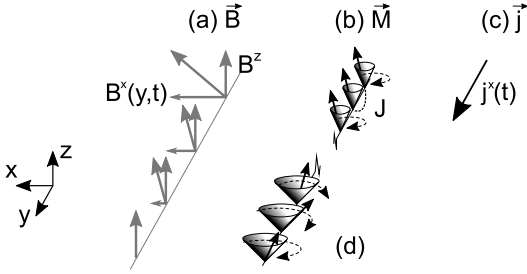


FIG. 1. Quasi-classical sketch of transverse spin transport in a spin chain directed along the  $y$ -direction: (a) External magnetic field with a static ‘bias’ component  $B^z$  and a perturbing, space- and time-dependent component  $B^x(y,t)$ ; (b)  $B^z$  produces a magnetization  $\vec{M}$  with a *homogeneous* transverse component and a Larmor precession,  $B^x(y,t)$  produces an *inhomogeneous* transverse component driving (c) a transverse spin-current  $j^x(y,t)$  in  $y$ -direction. The dynamics of  $j^x(y,t)$  is controlled by the intrinsic exchange coupling  $J$ . (d) As a function of time, the magnetization relaxes and the transverse component dephases.

Controlling quantum coherence is paramount for future information processing [1]. The coherence of localized quantum spin degrees of freedom has been studied in a wide variety of systems, including semiconductor quantum dots [2, 3], molecular magnets [4], nitrogen vacancies in diamond [5], carbon nanotubes [6], and ultracold atoms [7]. Coherence in spin transport has been addressed primarily in semiconductors [8]. A new route into coherent spin transport may arise from quantum magnets. Here, magnetization is transported solely by virtue of exchange interactions and (de)coherence of spins will emerge as a purely intrinsic many-body phenomenon. In one-dimensional (1D) spin systems, magnetic transport has experienced an upsurge of interest in the last decade due to the discovery of very large magnetic *heat* conduction [9] and long nuclear magnetic relaxation times [10]. Genuine *spin* transport in such materials remains yet to

be observed experimentally and if combined with materials with small exchange couplings [11, 12], the coherent manipulation of spin transport using laboratory magnetic fields may become feasible. Theoretically, spin transport has already been given significant attention (see Refs. 13 and 14 for a review), previous studies, however, have focused on the longitudinal spin conductivities only, excluding the physics of coherence. Therefore, in this Letter we investigate the dynamics of spin-currents with components transverse to an externally applied magnetic field, as sketched in Fig. 1. This setup allows us to study the collective precession frequency of the transverse spin-current and its decay time, which will be at the prime focus of this Letter. We will show that, besides a coherent oscillation at the Larmor frequency, a second nontrivial collective oscillation at higher frequencies emerges at low temperatures. This oscillation is identified as a pure many-magnon effect and also becomes coherent in the low temperature limit.

In this Letter, we study the antiferromagnetic Heisenberg spin chain, one of the fundamental models to describe magnetic properties of interacting electrons. It is relevant to the physics of low-dimensional quantum magnets [15], ultra-cold atoms [16], nanostructures [17], and - seemingly unrelated - fields such as string theory [18] and quantum Hall systems [19]. The Hamiltonian reads

$$H = J \sum_{r,\alpha} S_r^\alpha S_{r+1}^\alpha - B^z \sum_r S_r^z. \quad (1)$$

$S_r^\alpha$  ( $\alpha = x, y, z$ ) are the components of spin-1/2 operators at site  $r$ ,  $N$  is the number of sites,  $J > 0$  is the exchange coupling constant,  $B^z$  is a longitudinal magnetic field, and  $\hbar \equiv 1$  [20]. For  $B^z < B_C^z = 2J$ , Eq. (1) implies a gapless Luttinger liquid [21, 22] and, for  $B^z > B_C^z$ , a gapped ferromagnetic ground state.

We investigate the transverse spin-current dynamics for two complementary scenarios and use methods appro-

priate for each situation. First, we study current autocorrelations at finite temperature, using numerically exact diagonalization (ED) and an asymptotic analytic analysis (AAA). Second, applying the adaptive time-dependent density matrix renormalization group (tDMRG) [23], we analyze the real-time dynamics of currents at zero temperature during the evolution from initial states with an inhomogeneous magnetization. Qualitatively, the same physics explains our observations in both scenarios, and even a quantitative agreement can be obtained.

We begin by discussing the current autocorrelations  $\tilde{C}^{\mu\nu}(\omega) = \sum_{lm} e^{-\beta E_m} \langle l | j^\mu | m \rangle \langle m | j^\nu | l \rangle \delta(\omega - E_m + E_l) / ZN$  [24], where  $|l\rangle$ ,  $|m\rangle$  and  $E_{l,m}$  are eigenstates and -energies of Eq. (1),  $\beta = 1/T$  is the inverse temperature,  $j^\mu$  is the zero-momentum spin current,  $\mu, \nu = x, y, z$ ,  $Z$  is the partition function, and  $\omega$  is the frequency. More precisely, we consider a symmetrized version  $C^{\mu\nu}(\omega) = [\tilde{C}^{\mu\nu}(\omega) + \tilde{C}^{\mu\nu}(-\omega)]/2$ , i.e., in the time domain, we focus on the real part  $C^{\mu\nu}(t) = \text{Re}[\tilde{C}^{\mu\nu}(t)]$ . While  $B^z$  breaks total spin conservation, a spin-current can still be defined by decomposing the time derivative of the spin-density at momentum  $q$  as  $\partial_t S_q^\mu = \partial_t S_q^\mu|_{J=0} - \nu q j_q^\mu$  into a local source (sink) term due to  $B^z$  (present without any exchange interactions) and the actual exchange mediated spin-current  $j_q^\mu$ . The latter then derives from the continuity equation for  $S_q^\mu$  at  $B^z = 0$ . In turn  $\vec{j} = \nu \sum_r \vec{S}_r \times \vec{S}_{r+1}$ , where  $\vec{j} = \vec{j}_{q=0}$ . The eigenstates (energies) are classified according to the total spin  $z$ -component  $\sum_r S_r^z |l\rangle = M|l\rangle$ . Since  $|l\rangle$  is *independent* of  $B^z$  and  $C^{\mu\nu}$  is diagonal at  $B^z = 0$ , it will remain diagonal at any  $B^z$ . Moreover, by symmetry  $C^{xx} = C^{yy}$ . However, since  $j^x$  mediates transitions between sectors with  $\Delta M = \pm 1$  while  $j^z$  conserves  $M$ , the autocorrelations  $C^{xx}$  (transverse) and  $C^{zz}$  (longitudinal) *differ* at  $B^z \neq 0$ . This difference is solely due to the field dependence of the eigenenergies. Formally speaking, this aspect is at the center of this Letter. For the remainder we abbreviate  $C^{xx(zz)}$  by  $C^{x(z)}$ . Note that by the continuity equation the current autocorrelations at small  $q$  are related to the dynamic spin structure factor  $S^{\mu\nu}(q, \omega)$ , exhibiting a matrix symmetry identical to  $C^{\mu\nu}(\omega)$  at  $B^z \neq 0$  [25].

Generically, the longitudinal autocorrelation decomposes into a Drude weight  $D^z$  and a regular part, i.e.,  $C^z(\omega) = D^z \delta(\omega) + C_{\text{reg}}^z(\omega)$ . A significant body of evidence in favor of  $D^z(T \geq 0) \neq 0$  for  $B^z < B_c^z$  has been gathered [13, 14, 26], with thermally activated behavior of  $D^z(T)$  for  $B^z > B_c^z$  [14]. Less is known on the specific shape of the regular part [26]. The previous discussion of symmetries of  $C^{\mu\nu}$  implies that  $C^x(\omega) = \sum_{\pm} [D^x \delta(\omega \pm B^z) + C_{\text{reg}}^x(\omega \pm B^z)]$ . In general,  $D^x$  and  $C_{\text{reg}}^x$  will *not* be identical to  $D^z/2$  and  $C_{\text{reg}}^z/2$ , respectively, due to the different  $B^z$ -dependence of Boltzmann weights in  $C^z$  and  $C^x$ . In the time domain,  $D^x$  implies a coherent, nondecaying oscillation of the transverse current at the Larmor frequency  $\omega_L = B^z$ , permitted by

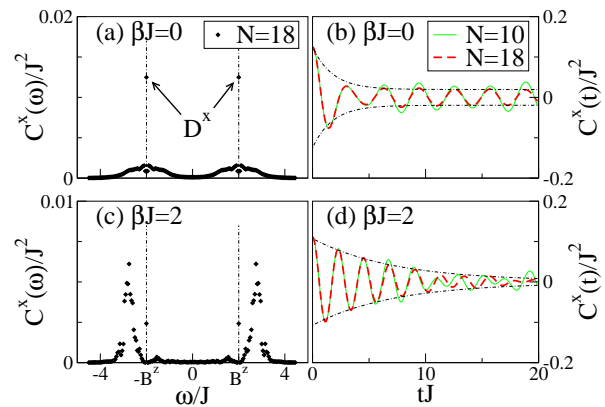


FIG. 2. (color online) Frequency and time dependence of the autocorrelation  $C^x$  for  $B^z/J = 2$  and (a), (b)  $\beta = 0$ , (c), (d)  $\beta J = 2$  (ED). The Drude weight in (a), (c) is visible exactly at the Larmor frequency  $\omega_L = B^z$  (vertical dashed-dotted lines). In (b), (d) the envelopes of fits [as defined in Eq. (3)] to data for  $N = 18$  are shown (dashed-dotted curves).

the integrability of Eq. (1) [13]. On the other hand,  $C_{\text{reg}}^x$  *a priori* implies only decoherence and damping. In the following, however, we demonstrate that at sufficiently low  $T$  and finite  $B^z$ , out of  $C^x$ , a new collective quasi-coherent oscillation of the current emerges. The oscillation frequency differs from the ‘simple’ Larmor frequency and cannot be understood within a one-magnon picture.

First, we discuss high temperatures, i.e.,  $\beta = 0$ . A straightforward analysis yields

$$C^x(\omega) = [C^z(\omega - B^z) + C^z(\omega + B^z)]/2. \quad (2)$$

Figure 2 (a) displays  $C^x(\omega)$  for  $B^z/J = 2$ . As can be seen from Fig. 2 (b), this approximately transforms into  $C^x(t) \approx [R(t) + D^x] \cos(\omega_L t)$  in the time domain, with  $R(t)$  *rapidly* decaying within  $\sim 1/\omega_L$  and a ‘trivial’ coherent oscillation due to the Drude weight.

Next we reduce the temperature to  $\beta J = 2$  at  $B^z/J = 2$ . Figure 2 (c) clearly shows two effects. First, the Drude weight  $D^x$  is strongly reduced. This reduction continues monotonously with increasing  $B^z$  (as discussed within the AAA below). Second, the regular part  $C_{\text{reg}}^x$  is strongly enhanced and undergoes an asymmetric weight redistribution with a major peak developing at a frequency  $\omega$  *larger* than  $\omega_L$  (and a minor peak at  $\omega < \omega_L$ ). This is consistent with  $B^z$  breaking particle-hole symmetry. In the time domain, see Fig. 2 (d), we find that

$$C^x(t) \approx R(t) \cos[(\omega_L + \delta\omega)t] + D^x \cos(\omega_L t) \quad (3)$$

allows for a reasonable leading-order fit of  $C^x(t)$  over several oscillation periods by assuming an exponential behavior  $R(t) = R_0 \exp(-t/\tau)$ , i.e., a single decay time  $\tau$ . In fact,  $C^x(\omega)$  is rather close to a Lorentzian in Fig. 2 (c). We find this approach to apply at least to  $B^z/J \leq 3$  and  $\beta J \leq 3$  and to have very little finite-size effects for the

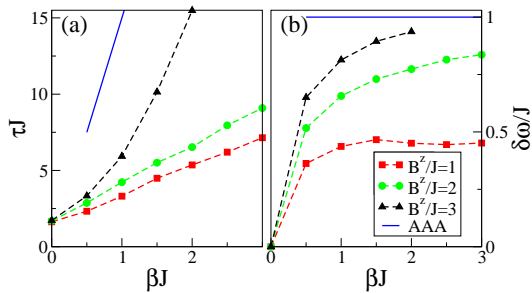


FIG. 3. (color online) (a) Decay time  $\tau$  and (b) frequency shift  $\delta\omega$  w.r.t.  $\beta$  for different  $B^z$ . Data are extracted from the autocorrelation  $C^x(t)$ , using ED for  $N = 18$  (symbols). Solid lines represent the low-temperature asymptote above the critical field, dashed curves are guides to the eye.

system sizes ( $N = 10, \dots, 18$ ) and time scales ( $tJ \leq 20$ ) studied [20]. Figure 2 (c) is a central result of this Letter. It unveils the emergence of a new collective frequency scale, namely at  $\omega_L + \delta\omega$ , in the transverse transport process besides the Larmor frequency. Moreover, for  $\tau \rightarrow \infty$  this process would be coherent.

In Fig. 3 we summarize our findings for  $\tau$  and  $\delta\omega$  over a range of temperatures and fields of  $0 \leq \beta J \leq 3$  and  $1 \leq B^z/J \leq 3$ . Figure 3 (a) shows that  $\tau$  increases roughly linearly with  $\beta$ , with an increasing slope as  $B^z$  increases. While finite system studies will not clarify if this result implies true coherence for a particular range of  $B^z$  as  $T \rightarrow 0$ , Fig. 3 (a) is at least strongly indicative of a large  $\tau$  in that limit. Regarding  $\delta\omega$ , Fig. 3 (b) clearly signals a saturation roughly at  $\beta J \sim B^z/J$  with the value at saturation increasing with  $B^z$ . We emphasize that  $\delta\omega \neq 0$  directly implies that the transverse current *cannot* be described in terms of transitions between the zero- and one-magnon sector. The dominant spectral weight of such one-magnon excitations at  $q = 0$  is exactly at  $\omega_L$  [25], leading to  $\delta\omega = 0$ .

To gain insight into the origin of  $\delta\omega \neq 0$  we present an AAA for  $B^z > B_c^z$  and low  $T$ . Here, the contribution of different  $M$ -sectors to  $C^x$  can be dissected asymptotically and, after an extensive analysis [20], we arrive at a simple picture: the transverse current is carried dominantly by transitions from the one-magnon sector around  $q \sim \pi$  into antibound states of the *two-magnon* continuum at the same  $q$ . The related frequencies  $\sim \omega_L + J$  and also the asymptotic form of  $C^x(t)$  can be obtained analytically:

$$C_{\text{AAA}}^x(t) \approx \sqrt{\frac{J^3}{\pi}} e^{-\beta(B^z - 2J)} \text{Re} \left( \frac{e^{i(\omega_L + J)t}}{\sqrt{2\beta + it}} \right). \quad (4)$$

This is consistent with Fig. 3 (b), which also suggests that  $\delta\omega \rightarrow J$  as  $B^z$  increases and  $\beta \rightarrow \infty$ . The thermal activation in Eq. (4) stems from the one-magnon energy at  $q = \pi$ . The damping results from summing over all transitions in the vicinity of  $q = \pi$  and its power-law behavior, i.e.  $\sim t^{-1/2}$ , for  $t \rightarrow \infty$  clearly shows that the single-scale

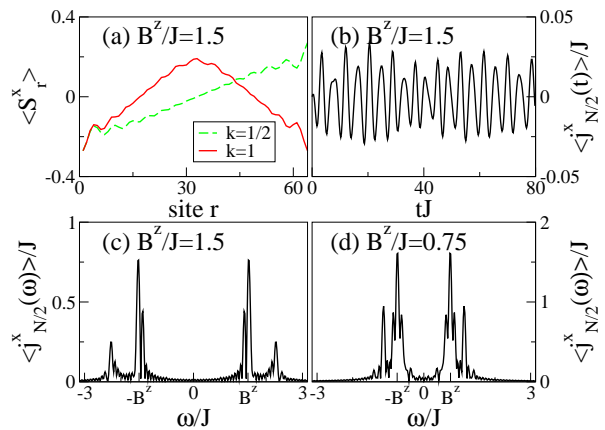


FIG. 4. (color online) Simulation of the transverse spin-current dynamics using tDMRG: (a) Initial magnetization profiles  $\langle S_r^x \rangle$  at  $t = 0$  for different  $k$ ; (b) Coherent oscillation of the spatially averaged current  $\langle j_{N/2}^x(t) \rangle$  for  $k = 0.5$  and  $B^z/J = 1.5$ ; (c), (d) Discrete Fourier transform for (b) and for  $B^z/J = 0.75$ . Besides the dominant peak at the Larmor frequency  $\omega_L = B^z$ , there is another significant peak at a higher frequency  $\omega_L + \delta\omega$ . For more details, see Ref. 20.

exponential used for  $R(t)$  in Eq. (3) is an approximation for not too low temperatures  $T$  only. Nevertheless, for a comparison with Fig. 3 (a), we extract a ‘decay time’ from the envelope of Eq. (4), i.e.  $|C_{\text{asy}}^x(t)/C_{\text{asy}}^x(0)| \leq 1/e$  for  $t \geq \tau$ , leading to  $\tau = 2\beta\sqrt{e^4 - 1} \approx 15\beta$ . As shown in Fig. 3 (a) (straight line), our ED data for  $B^z/J = 3$  are consistent with the asymptotic line, e.g., the slope  $d\tau/d\beta$  is already close to  $15\beta$  at  $\beta J \sim 2$ .

Now we turn to the real-time evolution of the spin-current derived from a Krylov-space based tDMRG approach [23]. This allows us to study larger systems than with ED, however, at zero temperature and only below the saturation field. The latter follows since there are no current-carrying states for  $B^z > B_c^z$  at  $T = 0$ . Moreover, since ED and AAA already suggest that  $\tau \rightarrow \infty$  as  $T \rightarrow 0$ , limitations in the accessible simulation times confine the tDMRG to an analysis of  $\delta\omega$ . To induce a current we add a perturbation  $H_1 = \sum_r B_r^x S_r^x$  to Eq. (1) with  $B_r^x = B^x \cos(2\pi kr/N)$ . First, the ground state of  $H + H_1$  is evaluated using DMRG, then the system is left to evolve under  $H$  alone.

Typical transverse magnetization profiles  $\langle S_r^x \rangle$  at  $t = 0$  are shown in Fig. 4 (a) for  $(B^z, B^x)/J = (1.5, 1)$  and for small values of  $k$ .  $\langle S_r^x \rangle$  follows  $B_r^x$  qualitatively, with additional  $2k_F$ -oscillations from the underlying Luttinger liquid. We perform the time evolution using  $m = 200$  states for the ground-state calculation, a time step of  $\delta t J = 0.25$ , and a fixed discarded weight [20, 23]. Although  $H_1$  breaks  $U(1)$  symmetry, we can still obtain reliable results for  $L \leq 64$  lattice sites. To analyze currents free of spatial oscillations we coarse-grain the data by averaging over suitable parts of the chain. Figure 4 (b) shows an example of the time evolution of the cur-

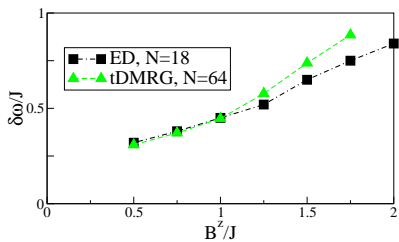


FIG. 5. (color online) Frequency shift  $\delta\omega$  w.r.t. the magnetic field  $B^z$ , as obtained from ED ( $\beta J = 3$ ) and tDMRG.

rent  $\langle j_{N/2}^x(t) \rangle$ , averaged over the left half of the chain, at  $(B^z, B^x)/J = (1.5, 1)$  for  $k = 0.5$ . For the times reached in the simulation ( $tJ \approx 80$ ), no relaxation can be observed. This is consistent with the expectation for  $T = 0$  drawn from ED and AAA. In view of the substantial number of periods covered in Fig. 4 (b) we have chosen to directly study the discrete Fourier transform of the real-time data in order to obtain the *dominant* frequencies. This is shown in Figs. 4 (c) and (d) for  $\langle j_{N/2}^x(t) \rangle$  at  $(B^z, B^x)/J = (1.5, 1)$  and  $(B^z, B^x)/J = (0.75, 1)$  at  $k = 0.5$ . These two figures clearly evidence the main result from tDMRG, namely that, fully consistent with the findings from ED and AAA, there are two characteristic frequencies in the current dynamics, namely  $\omega_L$  and  $\omega_L + \delta\omega$ . In contrast to the linear-response regime, the analysis of the relaxation scenario finds the contribution at  $\omega_L$  to be the larger one. This is not surprising since two different scenarios are compared, characterized by similar yet different correlation functions. We have checked that the results of Fig. 4 (b)-(d) are insensitive (i) to the details of the coarse-graining, (ii) to varying  $k$  within the small  $k$ -regime, and (iii) to the strength of  $B^x$ , at least up to  $B^x/J = 1$ , as used here [20]. The latter implies a minor role of non-linearity (non-equilibrium).

Finally, in Fig. 5 we compare  $\delta\omega$  from ED with tDMRG for  $0.5 \leq B^z/J \leq 2$ . The agreement is remarkably good indeed, not only in view of the different scenarios. For intermediate fields ( $B^z/J = 0.5, 0.75, 1$ ) the frequency shifts match each other almost exactly, while we attribute the slight deviation of ED from tDMRG at larger fields to finite temperature effects, where convergence to the  $T = 0$  values has not been reached yet [see  $B^z/J = 3$  in Fig. 3 (b)]. For  $B^z/J < 0.5$ , the accessible time scales prevent a reliable determination of  $\delta\omega$  in our approaches.

In summary, we studied the transverse spin-current dynamics in the spin-1/2 Heisenberg chain. As a main result, besides a coherent oscillation at the Larmor frequency, we provided evidence for a second nontrivial collective oscillation at higher frequencies, emerging at low temperatures as a genuine many-magnon effect and turning coherent as the temperature is lowered.

*Acknowledgments* This work was supported by the *Deutsche Forschungsgemeinschaft* through FOR 912.

## SUPPLEMENTAL MATERIAL

### I. Derivation of the Asymptotic Approximation

In this section we give a detailed derivation of the asymptotic approximation in Eq. (4) of the Letter. For convenience, we shift the zero point of the energy  $E$  to  $N(J/4 - B^z/2)$  and of the quantum number  $M$  to  $N/2$ . The shifted quantities will be denoted by  $\mathcal{E}$  and  $\mathcal{M}$  in the following,

$$\mathcal{E} = E - N\left(\frac{J}{4} - \frac{B^z}{2}\right), \quad \mathcal{M} = -\left(M - \frac{N}{2}\right). \quad (5)$$

Above the critical field the ground state is fully polarized

$$\psi_{(\mathcal{M}=0, q=0)} = |\uparrow\uparrow \dots \uparrow\uparrow\rangle \quad (6)$$

with momentum  $q = 0$  and energy  $\mathcal{E}_{(0,0)} = 0$ , see Fig. 6 (triangle). Periodic boundary conditions are assumed in this section. This state is an eigenstate of the current operator with the eigenvalue zero

$$j^x \psi_{(0,0)} = 0. \quad (7)$$

In the limit of  $T = 0$  only matrix elements from this initial state contribute to the current autocorrelation function  $C^x(\omega)$ . Therefore  $\lim_{T \rightarrow 0} C^x(\omega) = 0$ . At any finite temperature,  $\beta J \gg 1$ , initial states from the subspace with  $\mathcal{M} = 1$ , i.e. one-magnon states, start to contribute to the current autocorrelation function. Using the operator  $T^\mu$ , which translates a state by  $\mu$  sites, the eigenstates of the Hamiltonian  $H$  in Eq. (1) of the Letter read in this subspace

$$\psi_{(1,q)} = \frac{1}{\sqrt{N}} \sum_{\mu=0}^{N-1} e^{iq\mu} T^\mu |\downarrow\uparrow\uparrow \dots \uparrow\uparrow\rangle, \quad (8)$$

$q = 2\pi k/N$ ,  $k = 0, 1, \dots, N-1$ . Their energies are

$$\mathcal{E}_{(1,q)} = J(\cos q - 1) + B^z, \quad (9)$$

see Fig. 6 (crosses). At non-zero momentum these one-magnon states obviously carry a net-current, however, they are not eigenstates of the current operator. In fact one readily obtains

$$j^x \psi_{(1,q)} = i \frac{J}{2} (1 - e^{iq}) \varphi_{(2,q)}, \quad (10)$$

where  $\varphi_{(2,q)}$  are states from the subspace with  $\mathcal{M} = 2$ , i.e. the two-magnon subspace. They read

$$\varphi_{(2,q)} = \frac{1}{\sqrt{N}} \sum_{\mu=0}^{N-1} e^{iq\mu} T^\mu |\downarrow\downarrow\uparrow\uparrow \dots \uparrow\uparrow\rangle. \quad (11)$$

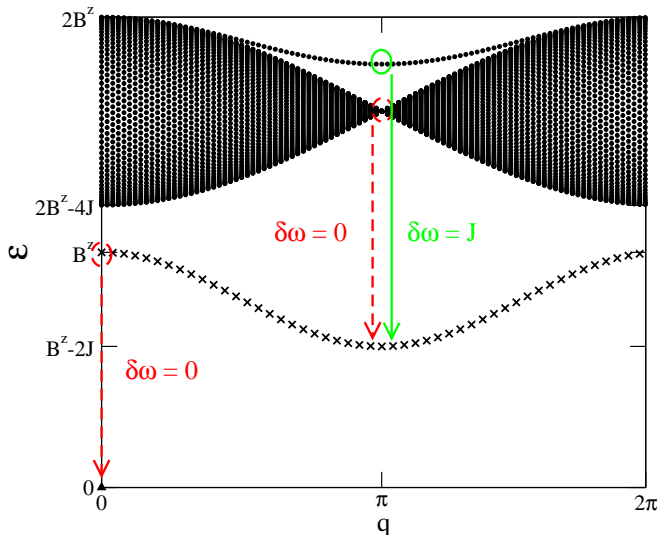


FIG. 6. The spectrum of the Hamiltonian in the  $\mathcal{M} = 0$ -, 1-, and 2-magnon subspaces (symbols). Additionally, those transitions of the transverse current are indicated that are relevant for the asymptotic approximation at low temperatures above the critical magnetic field: ‘Forbidden’ transitions (red, dashed lines) yielding no contribution as well as ‘allowed’ transitions (green, solid lines) leading to the dominant contribution. The latter transitions involve a two-magnon band at the edge of the Brillouin zone, i.e.,  $q = \pi$ . The associated frequencies are larger than the Larmor frequency  $\omega_L = B^z$ , namely, these frequencies are shifted by  $\delta\omega = J$ .

In general, and in contrast to Eqs. (8), (9), these states are *no* eigenstates of the Hamiltonian  $H$  in Eq. (1) of the Letter, but

$$H \varphi_{(2,q)} = (2B^z - J) \varphi_{(q,2)} + \frac{J}{2}(1 + e^{iq}) \tilde{\varphi}_{(2,q)}, \quad (12)$$

where  $\tilde{\varphi}_{(2,q)}$  refers to states generated by the transverse fluctuations of  $H$ , which separate the two adjacent flipped spins by one site. However, in the vicinity of  $q = \pi$ , the prefactor  $(1 + e^{iq})$  suppresses these contributions rendering  $\varphi_{(2,\pi)}$  an exact eigenstate of  $H$ . From its eigenenergy  $(2B^z - J)$  and Fig. 6 (green circle), it is obvious that this state is the (anti)bound two-magnon state  $\psi_{(2,q)}^r$  at  $q = \pi$ , well known from Bethe-Ansatz. Its dispersion over the complete Brillouin zone is [27]

$$\mathcal{E}_{(2,q)}^r = \frac{J}{2}(\cos q - 1) + 2B^z \quad (13)$$

and is situated above the two-magnon continuum.

Due to their Boltzmann weight the transitions from  $\psi_{(1,q)}$  into  $\varphi_{(2,\pi)}$  at  $q \approx \pi$  dominate the current autocorrelation function asymptotically for  $\beta J \gg 1$ . Therefore, the leading contribution to  $C^x$  results from projecting all intermediate states *solely* onto  $\psi_{(2,q)}^r$ . Since the anti-bound state is separated by a gap of  $\mathcal{O}(J)$  from the two-magnon continuum at  $q \approx \pi$ , we may use  $\langle \varphi_{(2,q)} | \psi_{(2,q)}^r \rangle \approx$

1 in that region, leading to

$$\tilde{C}_{\text{AAA}}^x(\omega) \approx \frac{1}{N} \sum_q e^{-\beta \mathcal{E}_{(1,q)}} |\langle \psi_{(1,q)} | j^x \psi_{(2,q)}^r \rangle|^2 \times \delta(\omega - [\mathcal{E}_{(2,q)}^r - \mathcal{E}_{(1,q)}]). \quad (14)$$

Using Eq. (10) and introducing the frequency  $\omega_q = J/2(1 - \cos q)$  this can be rewritten as

$$\tilde{C}_{\text{AAA}}^x(\omega) \approx \frac{J}{N} e^{-\beta B^z} \sum_q \omega_q e^{2\beta \omega_q} \delta(\omega - [B^z + \omega_q]). \quad (15)$$

Since momentum enters only through  $\omega_q$ , we may introduce the corresponding density of states and replace the sum by an integral with respect to  $\omega_q$ . This results in

$$\tilde{C}_{\text{AAA}}^x(\omega + B^z) \approx \frac{J}{2\pi} \frac{e^{\beta(2\omega - B^z)}}{\sqrt{J/\omega - 1}} \Theta(\omega) \Theta(J - \omega), \quad (16)$$

where  $\Theta(\omega)$  is the Heavyside function. Fourier transforming this to the time domain we get

$$\tilde{C}_{\text{AAA}}^x(t) \approx \frac{J^2}{2} e^{-\beta(B^z - J)} e^{i(B^z + J/2)t} \times \left[ \mathcal{I}_0\left(J\left[\beta + \frac{it}{2}\right]\right) + \mathcal{I}_1\left(J\left[\beta + \frac{it}{2}\right]\right) \right], \quad (17)$$

where  $\mathcal{I}_{0,1}(z)$  are modified Bessel functions of the first kind. At low temperatures, i.e. for  $\beta J \gg 1$ , we may insert their asymptotic forms for  $|z| \gg 1$ , which are  $\mathcal{I}_{0,1}(z) \approx e^z / \sqrt{2\pi z}$ . Therefore

$$\tilde{C}_{\text{AAA}}^x(t) \approx \sqrt{\frac{J^3}{\pi}} e^{-\beta(B^z - 2J)} \frac{e^{i(B^z + J)t}}{\sqrt{2\beta + it}}. \quad (18)$$

The real part of this, i.e.  $C_{\text{AAA}}^x(t) = \text{Re} \tilde{C}_{\text{AAA}}^x(t)$ , is Eq. (4) of our Letter, with  $\omega_L = B^z$ .

To assess the quality of the asymptotic approximation, we compare this result with ED for the current autocorrelation function above the saturation field, restricting the intermediate-state Hilbert space to two-particle states. This corresponds to taking the limit  $\beta J \gg 1$ . Due to this restriction ED is possible for rather large system sizes  $N$ . We choose  $N = 200$ . As shown in Fig. 7, the agreement is excellent. This validates the approximations involved in going from Eq. (10) to (18).

## II. ED Calculations

In this section we provide supplementary material on our ED calculations concerning a potential impact of the finite system size. Specifically, we demonstrate that for the systems of size  $N = 18$  and time scales  $tJ \lesssim 20$ , as used in the Letter, finite-size effects in the frequency shift  $\delta\omega$  and the relaxation time  $\tau$  can be neglected. *Both* of these quantities are determined by assuming a single

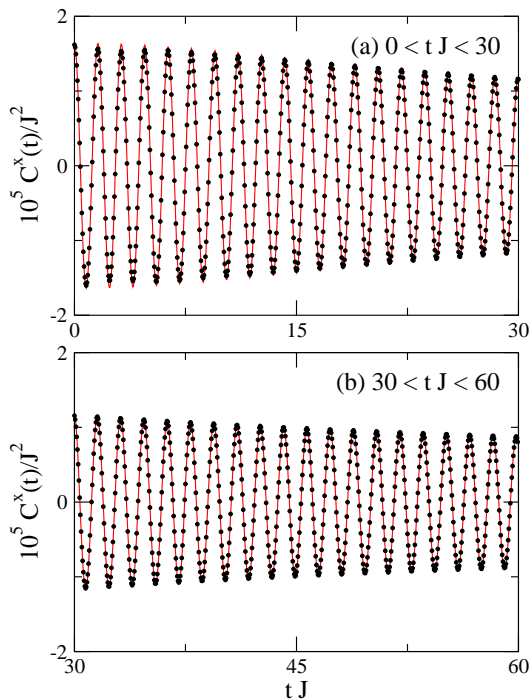


FIG. 7. The current autocorrelation function  $C^x(t)$  for (a)  $0 \leq tJ \leq 30$  and (b)  $30 \leq tJ \leq 60$ , restricted to the transitions into the subspaces  $\mathcal{M} \leq 1$  (one-magnon subspace). Data are evaluated numerically by the use of ED (circles) and are shown for the parameters  $\beta J = 9$ ,  $B^z/J = 3$ , and  $N = 200$ . For comparison, the asymptotic approximation according to Eq. (4) of the Letter is included (curves).

exponential  $R(t) = \exp(-t/\tau)$  to model the envelope of the decay of the coherent oscillation as in Eq. (3) of the Letter. This procedure leads to satisfactory fits to the ED results for not too low temperatures,  $\beta J \lesssim 3$ . Examples of this are shown in Fig. 2 of the Letter.

Figure 8 summarizes our results for  $\delta\omega$  and  $\tau$  as obtained from  $N = 10, 12, 14, 16$ , and  $18$  for various magnetic fields at  $\beta J = 2$ . This figure clearly demonstrates that both,  $\delta\omega$  and  $\tau$  either display almost no finite size dependence or a clear tendency towards saturation as a function of  $1/N$ . In all cases shown, the absolute changes in going from  $N = 16$  to  $18$  are negligible. Significant finite size effects can only be seen at systems sizes  $N \leq 14$ . Therefore, for the temperatures and fields considered in the Letter, it is justified to use  $N = 18$  data to obtain  $\delta\omega$  and  $\tau$  (see Fig. 3 of the Letter).

### III. DMRG Calculations

In this section we provide details of our DMRG simulations of the real-time evolution of the transverse current. We will focus on three aspects: (i) the coarse graining of the current, (ii) the dependence on the initial state and its characteristic wave length  $k$ , and (iii) the numerical

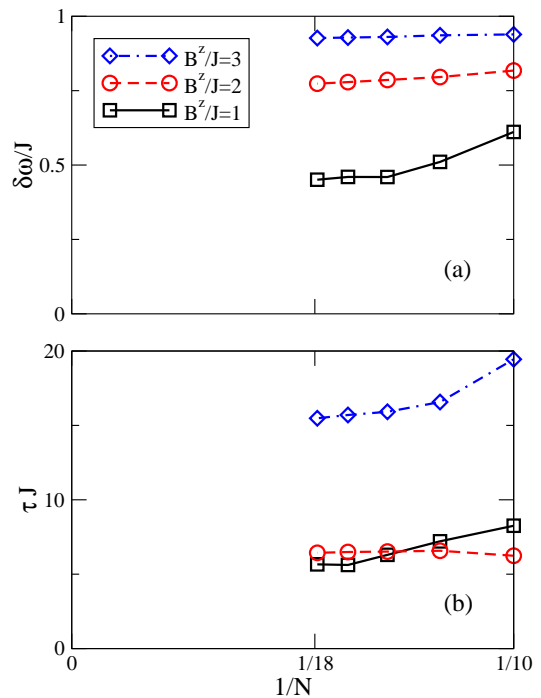


FIG. 8. The extracted (a) frequency shift  $\delta\omega$  and (b) decay time  $\tau$  as a function of the inverse size  $1/N$  for the parameters  $\beta J = 2$  and  $B^z/J = 1, 2$ , and  $3$  (symbols). Lines are guides to the eyes.

determination of the frequency shift  $\delta\omega$ , depending on the maximum simulation time and system size. The simulations were carried out with a fixed discarded weight, which we have varied from  $10^{-4}$  to  $10^{-6}$  in order to check convergence of our results.

Figure 9 shows the Fourier spectrum of the transverse current for two different coarse graining schemes. The solid, black line is taken from Fig. 4(c) of the Letter where we average the current over the left half of the chain (labeled by  $\alpha = N/2$  in Fig. 9). The dashed, red line is the result from averaging the current over five sites in the middle of the chain (denoted by  $\alpha = 5$ ); in this example, the coarse graining is taken over sites  $r = 30, 31, 32, 33, 34$  in a system with  $N = 64$ . As the figure clearly shows, the position of the two maxima, i.e., the one at the Larmor frequency  $\omega_L$  and the one at  $\omega_L + \delta\omega$ , as well as their (relative) weights are insensitive to the coarse graining.

Turning to the initial states of the real-time evolution, they are constructed by adding a site-dependent transverse field via a term  $\sum_r B_r^x S_r^x$  to the Hamiltonian with  $B_r^x = B^x \cos(2\pi kr/N)$ . Figure 10 illustrates that a central result of our Letter, namely the positions of the maxima in the current's Fourier spectrum, does not depend on the wave vector  $k$  of the perturbing field  $B_r^x$  in the long wave-length limit. Computational constraints lead to a decrease of the maximum simulation times accessible as  $k$  is increased. For a comparison of  $k = 1/2$  and  $1$

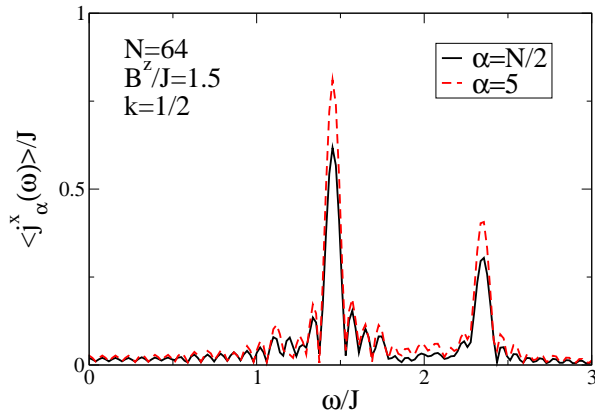


FIG. 9. Coarse graining: The solid, black line is the frequency-dependent current averaged over the left half of the system while the dashed, red line is averaged over five sites, counting away from the center of the system with  $N = 64$  (to be precise, these are sites  $r = 30, 31, 32, 33, 34$ ). The main features, i.e., the dominant frequencies do not depend on the coarse graining.

this implies that we have to confine ourselves to  $tJ \lesssim 40$ . Therefore, the features in Fig. 10 are broader than in Fig. 4 (c) of our Letter.

In Fig. 11, we address the convergence of the position of the second maximum in  $j_{N/2}^x(\omega)$  at  $\omega_L + \delta\omega$  as a function of the simulation time and the system size. Since we perform a discrete Fourier transform on a finite time window to obtain  $j_{N/2}^x(\omega)$  from the real-time data  $j_{N/2}^x(t)$ , the resulting spectrum depends on the maximum simulation time. After a minimum time needed to resolve the two frequencies has been reached we compute the spectrum after each time step and extract both frequencies. The quantity displayed in the figure is  $\omega_L + \delta\omega$  averaged over

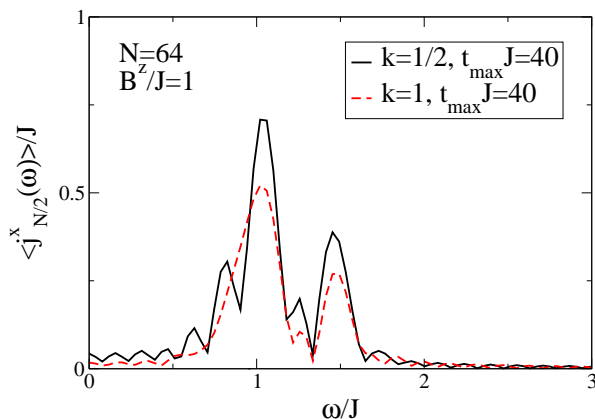


FIG. 10. Dependence on the initial state: Spectrum of the transverse current for two different values of  $k$ :  $k = 1/2$  (solid, black line) and  $k = 1$  (dashed, red line). In both cases,  $B^x/J = 1$ ,  $B^z/J = 1$  and  $N = 64$ . The Fourier transform is taken with  $t_{\max}J = 40$  due to the higher numerical costs at larger  $k$ .

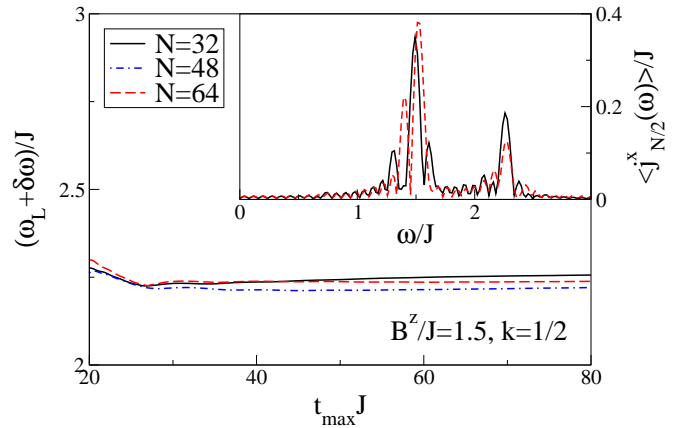


FIG. 11. Numerical determination of  $\omega_L + \delta\omega$  in dependence of the simulation time, for three different system sizes:  $N = 32$  (solid, black line),  $N = 48$  (dash-dotted, blue line) and  $N = 64$  (dash-dotted, red line). The final values are all within the overall numerical accuracy and no systematic finite size effects are visible. The inset shows the spectra at  $t_{\max}J = 80$  for  $N = 32$  (solid, black line) and  $N = 64$  (dashed, red line).

these spectra obtained from  $t_{\max}J = 20$  up to the maximum simulation time  $t_{\max}$ . For  $N = 32$  and  $48$  (solid, black and dash-dotted, blue line, respectively),  $\omega_L + \delta\omega$  weakly increases with  $t_{\max}$ , while for  $N = 64$  (dashed red line), the convergence is much faster. The finite-size effects in  $\omega_L + \delta\omega$  are non-monotonous and result in a small uncertainty of about 2-3%, well within the overall numerical accuracy of the simulations. The inset shows the spectrum of the current as a function of frequency at  $t_{\max}J = 80$  for  $N = 32$  and  $N = 64$ . While the dominant frequencies are only slightly affected by finite-size effects, spurious additional peaks appear on the smaller system that are irrelevant for the results and discussion presented in the Letter.

#### IV. Comment on Units

In the Letter all quantities are expressed in units of the exchange coupling constant  $J$ . Moreover, and to abbreviate the theoretical analysis, Planck's constant  $\hbar$  has been set to unity as usual. Similarly, the Bohr magneton  $\mu_B$  and the spin Landé factor  $g_S$  have been absorbed into the definition of the magnetic field. The correspondence between these units and SI-units is summarized in Tab. I. Therein,  $J$  is expressed in units of temperature, i.e., divided by the Boltzmann constant  $k_B$ .

\* r.steinigeweg@tu-bs.de

[1] J. Fischer and D. Loss, Science **324**, 1277 (2009).  
[2] D. J. Reilly *et al.*, Science **321**, 817 (2008).

quantity	unit	
	Letter	SI
magnetic field	$J$	$k_B/(\mu_B g_S) (J/k_B)$ $\approx 0.744 \text{ T/K} (J/k_B)$
frequency	$J$	$k_B/\hbar (J/k_B)$ $\approx 1.309 \cdot 10^{11} \text{ Hz/K} (J/k_B)$
time	$1/J$	$\hbar/k_B (k_B/J)$ $\approx 7.638 \cdot 10^{-12} \text{ sK} (k_B/J)$

TABLE I. Correspondence between the units in the Letter and SI-units.

- [3] S. Foletti *et al.*, Nature Phys. **5**, 903 (2009).  
[4] A. Ardavan *et al.*, Phys. Rev. Lett. **98**, 057201 (2007).  
[5] G. Balasubramanian *et al.*, Nature Mat. **8**, 383 (2009).  
[6] H. O. H. Churchill *et al.*, Phys. Rev. Lett. **102**, 16682 (2009).  
[7] J. Beugnon *et al.*, Nature Phys. **3**, 696 (2007).  
[8] Y. Kato *et al.*, Nature **427**, 50 (2004); B. Huang, D. J. Monsma, and I. Appelbaum, Phys. Rev. Lett. **99**, 177209 (2007); N. P. Stern *et al.*, Nature Phys. **4**, 843 (2008).  
[9] A. V. Sologubenko *et al.*, Phys. Rev. Lett. **84**, 2714 (2000); C. Hess *et al.*, Phys. Rev. B **64**, 184305 (2001); N. Hlubek *et al.*, Phys. Rev. B **81**, 020405 (2010).  
[10] K. R. Thurber *et al.*, Phys. Rev. Lett. **87**, 247202 (2001).  
[11] M. Klanjšek *et al.*, Phys. Rev. Lett. **101**, 137207 (2008).  
[12] H. Kühne *et al.*, Phys. Rev. B **80**, 045110 (2009).  
[13] X. Zotos and P. Prelovšek, *in: Transport in one dimensional quantum systems* (Kluwer Academic Publishers, Dordrecht, 2004).  
[14] F. Heidrich-Meisner, A. Honecker, and W. Brenig, Eur. Phys. J. Special Topics **151**, 135 (2007).  
[15] D. C. Johnston *et al.*, Phys. Rev. B **61**, 9558 (2000).  
[16] S. Trotzky *et al.*, Science **319**, 295 (2008).  
[17] P. Gambardella, Nature Mat. **5**, 431 (2006).  
[18] M. Kruczenski, Phys. Rev. Lett. **93**, 161602 (2004).  
[19] Y. B. Kim, Phys. Rev. B **53**, 16420 (1996).  
[20] See Sec. Supplemental Material or <http://link.aps.org/supplemental/10.1103/PhysRevLett.106.160602> for more details.  
[21] R. B. Griffiths, Phys. Rev. **133**, A768 (1964).  
[22] F. D. M. Haldane, Phys. Rev. Lett. **45**, 1358 (1980).  
[23] A. J. Daley *et al.*, J. Stat. Mech.: Theor. Exp. **2004**, P04005; S. R. White and A. E. Feiguin, Phys. Rev. Lett. **93**, 076401 (2004); G. Vidal, Phys. Rev. Lett. **93**, 040502 (2004).  
[24] G. D. Mahan, *Many particle physics* (Plenum Press, New York, London, 1980).  
[25] S. Grossjohann and W. Brenig, Phys. Rev. B **79**, 094409 (2009).  
[26] For  $M > 0$ ,  $D^z(T > 0) > 0$  [13]. The  $M = 0$  case is still under scrutiny: see J. Sirker, R. G. Pereira, and I. Affleck, Phys. Rev. Lett. **103**, 216602 (2009); S. Grossjohann and W. Brenig, Phys. Rev. B **81**, 012404 (2010); Refs. [13, 14], and references therein.  
[27] H. Bethe, Z. Phys. A **71**, 205 (1931).